

# Optical band-gap and associated Urbach energy tails in defected AlN thin films grown by ion beam sputter deposition: Effect of assisted ion energy

Neha Sharma\*, K. Prabakar, S. Ilango, S. Dash, A. K. Tyagi

*Material Science Group, Indira Gandhi Centre for Atomic Research, Kalpakkam 603102, TN, India*

\*Corresponding author, Tel: (044) 27480500-22086; E-mail: neha@igcar.gov.in

Received: 30 March 2016, Revised: 30 September 2016 and Accepted: 14 April 2017

DOI: 10.5185/amp.2017/511  
www.vbripress.com/amp

## Abstract

AlN thin films were grown by ion beam sputter deposition in reactive assistance of  $N^+/N_2^+$  ions on Si (100) substrates. During deposition, assisted ion energy ( $E_A$ ) was varied as 90 eV and 120 eV with a post deposition exposure to  $N_2$  plasma. The resultant films were characterized by grazing incidence x-ray diffraction (GIXRD) for their structure and atomic force microscopy (AFM) for their root mean square (rms) surface roughness ( $\delta$ ). UV-VIS spectrophotometry was carried out to explore their optical band-gap with associated Urbach ( $E_U$ ) and weak absorption tail ( $E_{WAT}$ ) energies. Our results show that, AlN thin film grown with 90 eV reactive ion assistance possesses larger optical band gap ( $E_g$ ) of 5.3 eV associated with comparatively narrower band tails when compared to those AlN thin film samples which were grown for 120 eV reactive ion assistance. These optical band-gaps are further correlated with corresponding Urbach energy tails which can be used as a measure of disorder in microstructure of the film. Also, appropriate optimization of energy tails substantiates the possibility of band gap engineering as per the requirement of different thin film devices. Copyright © 2017 VBRI Press.

**Keywords:** Ion beam sputter deposition, reactive assistive mode, AlN thin films, optical band-gap, Urbach energy tail.

## Introduction

Wide band gap semiconductor materials have become the subject of intense study due to their potential applications in the field of thin film devices. For non-destructive testing (NDT) including, object recognition, ranging and velocity sensing and medical imaging, ultrasonic transducers have been proven to be of great utility [1-3]. Conventionally, bulk piezoelectric ceramics are used as ultrasonic transducers. But their main drawback is poor acoustic coupling to air or water. Also, they are expensive to machine into 2D transducer arrays which are needed for 3D imaging [4, 5]. To overcome these difficulties, microelectromechanical system (MEMS) based ultrasonic transducers have emerged as a promising candidate. This micromachined structures offer easy fabrication of larger 2D arrays that enable high resolution real time measurement capabilities. Among two main MEMS technologies which are in practice for the miniaturization of micromachined ultrasonic transducers are piezoelectric and capacitive technologies [6]. Piezoelectric thin film technology presents more advantages over capacitive technology like low actuation

voltage (1-10V), compatibility with complementary metal oxide semiconductor (CMOS) technology and/or easy integration on flexible substrates. Most investigated piezoelectric materials for the application in the field of piezoelectric ultrasonic transducers (PUTs) are lead zirconate titanate (PZT), zinc oxide (ZnO) and aluminum nitride (AlN). Use of AlN thin films is more advantageous over other mentioned materials due to its moderate piezoelectric response with wide band-gap and superior dielectric properties. Generally, AlN crystallizes in the wurtzite hexagonal structure and exhibits excellent thermal conductivity, good electrical insulation characteristics and a coefficient of thermal expansion closely matching that of silicon (Si) [7]. But at the same time, due to low intrinsic carrier concentration, presence of deep native defects and impurity energy levels, the electrical characterization of AlN thin films has been difficult. In view of this, UV-VIS spectrophotometry offers an easy and reliable way of investigating the band gap of AlN thin films.

Based upon many device specific requirements, there are several deposition techniques by which such AlN thin films can be grown on various substrates [8, 9]. But

reactive ion beam sputter deposition (IBSD) is a specialized technique for the deposition of device quality thin films. Thus, AlN thin films grown by IBSD must be characterized to evaluate their optical band gap over a wide range of wavelength ( $\lambda$ ) at different deposition parameters such as substrate temperature, assisted ion energy and current. Also, optical band-gap of AlN thin films can easily be tailored by introducing defects in its microstructure in assistive mode of IBSD. The disorder thus created and its effect on the band-gap can be understood in terms of Urbach energy tails. Knowledge of its optical band-gap and corresponding Urbach energy tails can then judiciously be used to tailor their band-gap to a desired value.

In the present study, the role of different assisted ion energy on the evolution of its optical band-gap is addressed by assessing Urbach energy tail. Grazing-incidence x-ray diffraction (GIXRD) and atomic force microscopy (AFM) were used to understand their structural and morphological evolution.

## Experimental

### Material synthesis

AlN-thin films were grown by IBSD on Si (100) substrate. The deposition chamber of IBSD system is equipped with an RF ion source which can be operated to extract the inert gas ions in the range 100eV – 2KeV. Usually, ultra-high pure (UHP) argon (Ar) gas is used to feed RF ion source and Ar<sup>+</sup> ions are extracted to sputter the target. An end-Hall type grid less ion source is used to extract the flux of reactive ions in the energy range of 50eV - 180 eV to assist the sputter deposition process [10]. To deposit AlN thin films, UHP nitrogen (N<sub>2</sub>) gas was fed into the assistive ion source to extract N<sup>+</sup>/N<sub>2</sub><sup>+</sup> ions for reactive deposition. Prior to deposition of AlN-thin films, main chamber was pumped down to a base pressure of 4x10<sup>-7</sup> mbar while working pressure was maintained at 3x10<sup>-4</sup> mbar. During deposition, metal atom flux was supplied by sputtering aluminum (Al) target (99.999% pure) with Ar<sup>+</sup> ion beam of 500 eV and 40mA current. Simultaneously, reactive flux of N<sup>+</sup>/N<sub>2</sub><sup>+</sup> ions were provided by assisted ion source at two different energies, 90 eV and 120 eV keeping current constant at 200mA. Each deposition was carried out for 40 minutes. In each case films were exposed to the reactive flux of N<sup>+</sup>/N<sub>2</sub><sup>+</sup> ions for 5 minutes after deposition with respective assisted energy. The samples thus grown are designated as T90 and T120 respectively. Thickness of these thin films was measured using a surface profilometer (VEECO, USA) which was found to be 50.6 nm and 34.4 nm respectively for T90 and T120.

### Characterization

X-ray diffraction (XRD) was used to explore the crystal structure of reactive assistive IBSD grown AlN thin films. GIXRD measurements (Bruker D8, Germany) were carried out to explore their structure at incident angles of

0.5° in the steps of 0.001° in the 2 $\theta$  angular range of 10° to 90° for both T90 and T120. As relevant information could be obtained in the 2 $\theta$  range of 40° to 50°, GIXRD plots are displayed in this range only. Furthermore, surface morphology of these AlN thin films was analyzed using AFM (NT-MDT, Russia) in semi-contact mode. To determine the optical band-gap ( $E_g$ ) of these AlN thin films UV-VIS spectrophotometer (Jasco V650, Japan) was investigated. The optical system under investigation is considered as a binary system constituted by a thin and homogeneous film of AlN deposited on opaque Si (100) substrate. Thickness of the substrate is kept much higher than the film. The electromagnetic radiation was incident upon the film surface in near normal incidence and diffused reflectance spectra were collected for both the samples in the wavelength ( $\lambda$ ) range of 200 - 900 nm.  $E_g$  was obtained by obtaining Tauc plots in the corresponding region of absorption coefficient ( $\alpha$ ) vs.  $\lambda$  curves. Associated Urbach energy tails were also calculated by analyzing the  $\ln(\alpha)$  vs.  $E(h\nu)$  curves to determine the possible constitution of AlN thin film band-gap.

## Results and discussion

**Fig. 1** shows the GIXRD patterns obtained for T90 and T120 AlN thin film samples. It can be observed from **Fig. 1(a)**, that for 90 eV assistance of N<sup>+</sup>/N<sub>2</sub><sup>+</sup> ions, formation of cubic polytype of AlN (C-AlN) takes place. As the assistive ion energy is increased to 120 eV, the microstructure of AlN thin film changes into amorphous state. This is shown in **Fig. 1(b)**.

Thus it can easily be understood that 90 eV assistance of N<sup>+</sup>/N<sub>2</sub><sup>+</sup> ions is the optimum energy to deposit crystalline phase of AlN. Subsequently, surface morphology of T90 and T120 are investigated using an AFM. For T90, lower surface roughness is observed with an root mean square (rms) value ( $\delta$ ) of 1.4 nm. At the same time, for the film T120 grown with higher energy assistance, larger value of  $\delta = 3.4$  nm is obtained. As smooth surface is the primary requisite for thin film device fabrication, AlN thin film sample T90 is found to be more suitable for device applications.

In case of thin film PUTs, band-gap of the material used for piezoelectric activity becomes important. Wide band gap AlN thin film has several characteristics that make them more useful when compared to other piezoelectric materials with lower band gap. Wide band gap of AlN enables the thin film PUTs to operate at higher temperature. It also allows devices to operate at much higher voltages and currents. Thus it becomes necessary to investigate the band gap of reactive assistive IBSD grown AlN thin films at different assisted ion energy ( $E_A$ ). In this context, the diffused reflectance spectra for T90 and T120 were obtained using a UV-VIS spectrophotometer which are analysed to obtain the absorption coefficient ( $\alpha$ ) vs.  $h\nu$  plots.

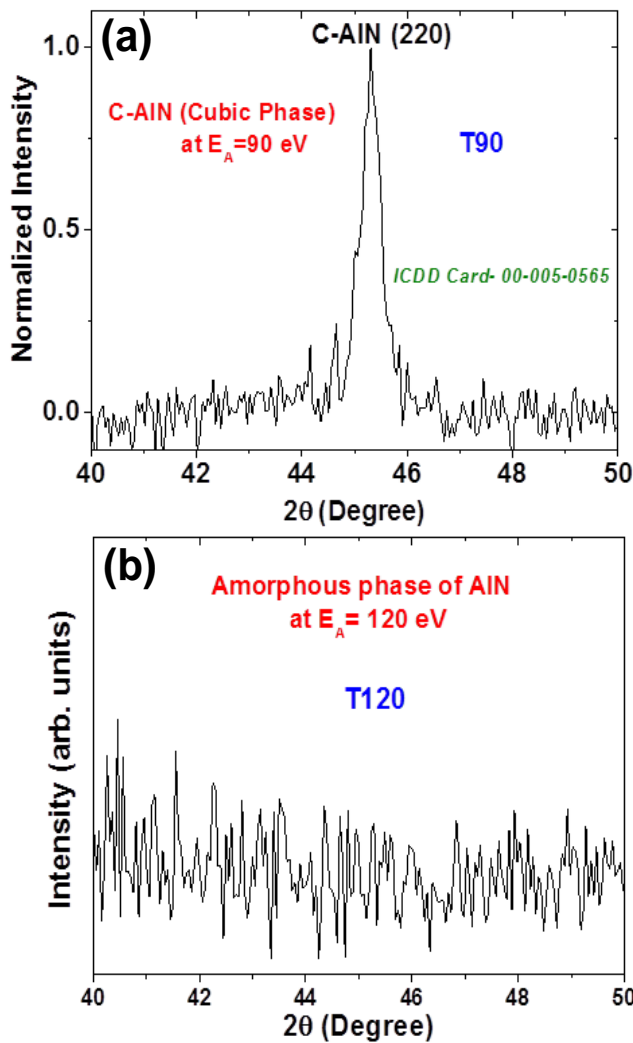


Fig. 1. Grazing incidence x-ray diffraction (GIXRD) patterns for the AlN thin films obtained at (a) 90 eV (T90) assistance and (b) 120 eV (T120) assistance of N<sup>+</sup>/N<sub>2</sub><sup>+</sup> ions.

Fig. 2 and 3 show the  $\alpha$  vs.  $h\nu$  plots obtained for AlN thin film samples T90 and T120 respectively. These plots can be divided into three regions for analysis. First region belongs to weak absorptions which is designated as *weak absorption tail region* (WAT-Region). It represents those transitions which take place from one localized tail state above the valence band to another localized tail state below the conduction band and/or from one localized tail state below the conduction band to another localized tail state above the valence band. In this WAT-region,  $\alpha$  follows  $h\nu$  according to following relation [11]:

$$\alpha(h\nu) = \alpha_o \exp\left(\frac{h\nu}{E_{WAT}}\right) \quad (1)$$

Where  $\alpha_o$  is a constant, ' $h\nu$ ' is the photon energy and  $E_{WAT}$  represents the weak absorption tail energy.

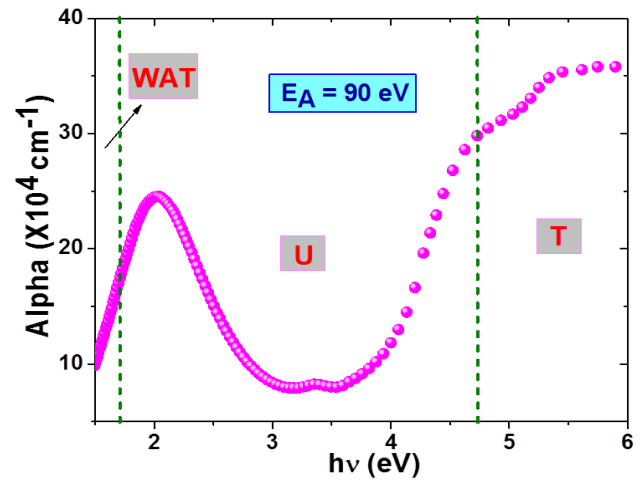


Fig. 2 Variation of absorption coefficient ( $\alpha$ ) of AlN thin film, grown with 90 eV N<sup>+</sup>/N<sub>2</sub><sup>+</sup> ion assistance, with incident photon energy ( $h\nu$ ).

Generally in optical absorption, an electron from the top of the valence band gets excited into the bottom of the conduction band across the energy band gap [12]. During this transition process, if some disorder is generated due to the presence of localized tail states originated from the presence of defects in film microstructure, the density of electronic states in valence and conduction band tails into the energy gap.

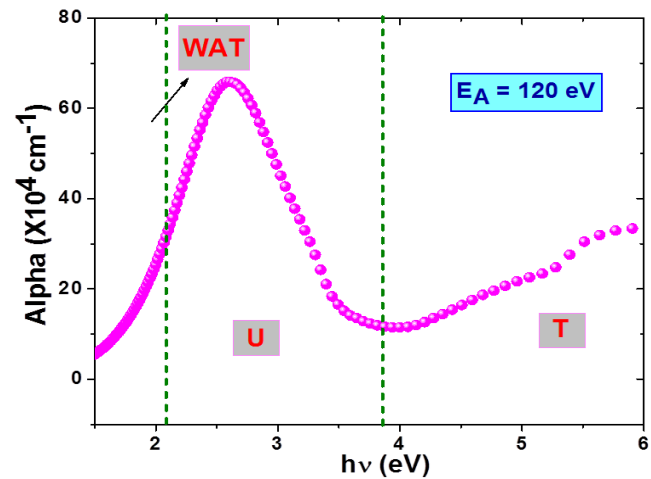


Fig. 3. Variation of absorption coefficient ( $\alpha$ ) of AlN thin film, grown with 120 eV N<sup>+</sup>/N<sub>2</sub><sup>+</sup> ion assistance, with incident photon energy ( $h\nu$ ).

This tail of density of electronic states extending into the energy band gap is called as Urbach tail. Consequently, absorption coefficient  $\alpha(h\nu)$  also tails off exponentially and energy represented by these localized tail states is referred to as Urbach energy. This is represented by the *Urbach region* (U-region) in Figs. 2 and 3. This region represents those electron transitions which take place from one extended valence band state to another tail state below the conduction band and/or from one extended conduction band state to another tail state above the valence band.  $E_U$  can be calculated by the following equation [11]:

$$\alpha(h\nu) = \alpha_0 \exp\left(\frac{h\nu}{E_U}\right) \quad (2)$$

where,  $\alpha_0$  is a constant, ' $h\nu$ ' is the photon energy and  $E_U$  is the Urbach energy [11, 12]. In general, band-gap is obtained from the optical absorption edge energy. This is the minimum photon energy required to excite an electron from the highest occupied molecular orbital (HOMO) at the top of the valence band to the lowest unoccupied molecular orbital (LUMO) at the bottom of the conduction band. Thus Tauc-region (T-region) in Fig. 2 and 3 represent those transitions which take place between the extended valence band state to extended conduction band state across the band-gap. Generally, two types of transitions can take place at this fundamental edge: direct and indirect transitions. Both of these transitions involve the interaction of an electromagnetic wave with an electron in the valence band which gets excited into the conduction band across the fundamental band gap [11, 12]. However, in case of indirect transition, simultaneous interaction with lattice vibration also takes place. In the light of this, the form of the absorption coefficient  $\alpha$  can be described by the relation,

$$(\alpha h\nu)^{1/n} \sim A(h\nu - E_g) \quad (3)$$

where,  $E_g$  is the optical band gap,  $A$  is a proportionality constant and  $n$  takes different values corresponding to different transitions [12]. Since AlN is known as a direct band-gap material, we take  $n = 1/2$  for direct allowed transition. All these three types of transitions are schematically represented in Fig. 4 for better understanding.

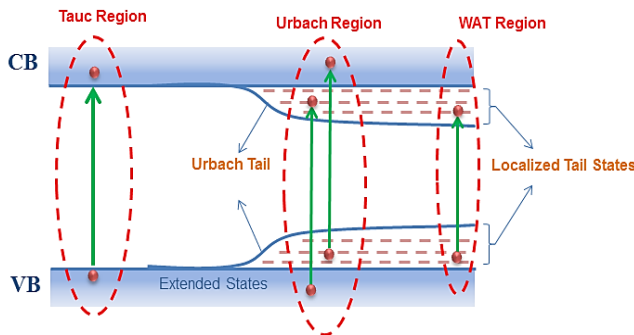


Fig. 4. Schematic representation of various transitions between valence band (VB) and conduction band (CB). Tauc region, Urbach region and weak absorption tail region are highlighted with dotted circles.

Fig. 5 shows the Tauc's plot obtained for AlN thin film sample T90. It was obtained from T-region of the figure 2 as it represents the longest transition. To obtain the value of  $E_g$ , linear portion of the  $(\alpha h\nu)^2$  vs.  $h\nu$  curve is fitted with a straight line and then extrapolated back to the horizontal axis. Value of  $h\nu$  where extrapolated linear fit intersects the horizontal axis is taken as  $E_g$ . For thin film sample T90,  $E_g = 5.3$  eV is obtained using equation (3).

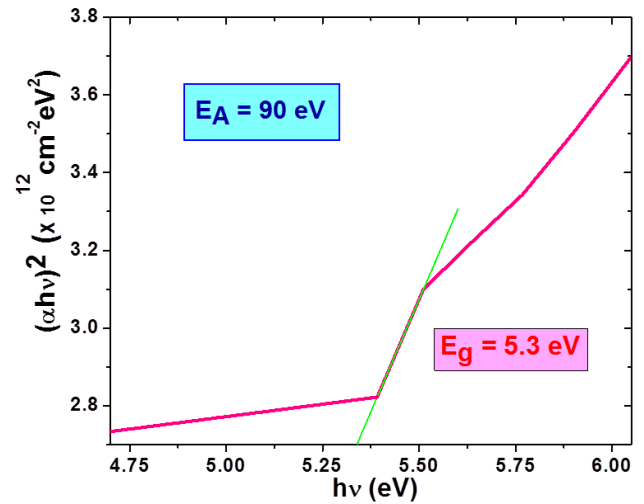


Fig. 5. Tauc plot for sample T90 gives the optical band-gap ( $E_g$ ) of 5.3 eV.

Similarly, for AlN thin film sample T120, Fig. 6 shows that  $E_g = 4.9$  eV. This indicates clearly that with a 90eV assistance of  $N^+/N_2^+$  ions, efficient formation of AlN takes place with lesser incorporation of defects. While during 120 eV  $N^+/N_2^+$  ion assistance, the  $E_g$  becomes narrower. Ion beam assisted deposition is well-known to generate near surface defects during deposition process [10]. Thus the reduction in  $E_g$  for T120 can be attributed to the incorporation of more localized states due to incorporation of defects from continuous exposure of  $N^+/N_2^+$  ions of higher energy.

Table 1 Optical band gap ( $E_g$ ), Urbach tail energy ( $E_U$ ) and weak absorption tail energy ( $E_{WAT}$ ) values obtained for T90 and T120.

AlN Thin Film Sample	$E_g$ (eV)	$E_U$ (eV)	$E_{WAT}$ (eV)
90	5.3	0.576	0.333
T120	4.9	0.779	0.380

In view of the above discussion, values of  $E_{WAT}$  and  $E_U$  are calculated from equations (1) and (2). The Weak absorption and Urbach energy tail is estimated by plotting  $\ln(\alpha)$  vs.  $h\nu$  taking  $\alpha$  in the range of WAT and U-region. Fitting the linear portion of the curve with a straight line, the reciprocal of the slope yields the value of  $E_{WAT}$  and  $E_U$ . These values are listed in Table 1. It can be noticed here that for sample T90, smaller band tailing with  $E_U = 0.576$  eV and  $E_{WAT} = 0.333$  eV is observed. As the energy of the reactive assistive flux of  $N^+/N_2^+$  ions is increased to 120 eV for T120, incorporation of more number of localized defect states widens the band tails having values  $E_U = 0.779$  eV and  $E_{WAT} = 0.380$  eV. This clearly indicates that larger is the band tail energy ( $E_U + E_{WAT}$ ), narrower is the  $E_g$ .

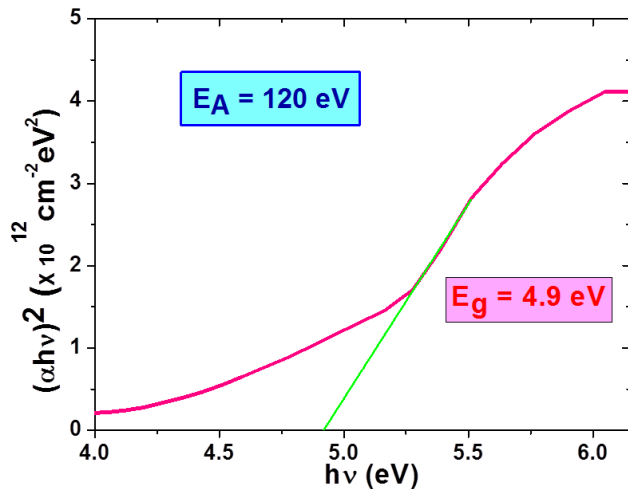


Fig. 6. Tauc plot for sample T120 gives the optical band-gap ( $E_g$ ) of 4.9 eV.

## Conclusion

AlN thin films were deposited on Si(100) substrate by reactive assistive IBSD at different assisted ion energy of 90 eV and 120 eV with post deposition exposure to  $N^+/N_2^+$  flux for 5 minutes. GIXRD measurements confirmed that the film deposited with 90 eV  $N^+/N_2^+$  ion assistance possess cubic crystal structure. While film deposited with 120 eV  $N^+/N_2^+$  ion assistance was amorphous in nature. AFM measurements indicated the increase in the rms roughness from 1.4 nm to 3.4 nm as the assisted ion energy was increased from 90 eV to 120 eV. Diffused reflectance measurements were carried out at ambient conditions in the wavelength range of 200 – 900 nm. The  $\alpha$  vs.  $h\nu$  curve thus obtained was analysed by dividing into three regions. The optical band-gap of the films was estimated by Tauc plot obtained in the region-T while weak absorption and Urbach energy tails were calculated in region-WAT and region-U, respectively. For 90 eV assistance of  $N^+/N_2^+$  ions, optical band-gap was found to be 5.3 eV. But for 120 eV  $N^+/N_2^+$  ion assistance, optical band-gap was reduced to 4.9 eV. These observations were further substantiated by estimating the weak absorption and Urbach energy tailing into the band-gap in each case. These energy tails can judiciously be optimized to engineer the optical band gap for various applications in the field of thin film devices.

## Acknowledgements

The authors would like to thank Dr. G. Amarendra, Director, Materials Science Group for his encouragement and support. The authors also would like to acknowledge Ms. Sunitha Rajkumari for XRD measurements.

## Author's contributions

Conceived the plan: Neha Sharma; Performed the experiments: Neha Sharma, K. Prabakar; Data analysis: Neha Sharma; Wrote the paper: Neha Sharma, S. Ilango, S. Dash, A. k. Tyagi. Authors have no competing financial interests.

## References

1. Lu Y., Shelton, S., and Horsley, D. A., Solid-State Sensors, Actuat. Microsyst. Workshop, Hilton Head, SC, USA, 2014,131.
2. Lu, Y., Heidari, A., Shelton, S., Guedes, A., Horsley, D. A., IEEE 27th MEMS, San Francisco, CA, USA, 2014, 745.
3. Griffin, B., A., Williams, M. D., Coffman, C. S., Sheplak, M.; J. Microelectromech. Syst., 2011, 20, 476.
4. Mastronardi, V. M., Guido, F., Amato, M., Vittorio, M. D., Petroni, S.; Microelectron. Eng., 2014, 121, 59
5. Lu, Y., Horsley, D. A.; J. of Microelectromech. Syst., 2014, 27th in Proc. IEEE 27th MEMS, USA, 2015, 1.
6. Ghodssi, R., Lin, P., (Eds.), MEMS Materials and Processes Handbook; Springer: USA, 2011.
7. Ho, C., J., Shing, t., K., Li, P. C.; Tamkang J. of Sci. and Eng., 2004, 7, 1.
8. Cappelli, E., Trucchi, D. M., Orlando, S., Valentini, V., Mezzi, A., Kaciulis, S.; Appl. Phys. A, 2014, 114, 611.
9. Takahashi, K., Yoshikawa, A., Sandhu, A. (Eds.), Wide Bandgap Semiconductors: Fundamental Properties and Modern Photonic and Electronic Devices, Springer: USA, 2007.
10. Sharma, N., Prabakar, K., Ilango, S., Dash, S., Tyagi, A. K.; Appl. Surf. Sci., 2015, 347, 875
11. Singh, J., (Eds.), Optical Properties of Condensed Matter and Applications, Wiley: 2006
12. Adachi, S., (Eds.), Optical Properties of Crystalline and Amorphous semiconductors: Materials and Fundamental Principles, Springer, New York, 1999.